Waste Management 106 (2020) 226–239

Contents lists available at ScienceDirect

Waste Management

journal homepage: www.elsevier.com/locate/wasman

Real time monitoring of slow pyrolysis of polyethylene terephthalate (PET) by different mass spectrometric techniques

Asma Dhahak [a], Christoph Grimmer [b], Anika Neumann [b], Christopher Rüger [b], Martin Sklorz [b,c], Thorsten Streibel [b,c], Ralf Zimmermann [b,c], Guillain Mauviel [a], Valérie Burkle-Vitzthum [a,*]

[a] Laboratory of Reactions and Process Engineering (LRGP), National Centre for Scientific Research (CNRS), University of Lorraine, National School of Chemical Industries (ENSIC), 1 Rue Grandville, 54000 Nancy, France
[b] Joint Mass Spectrometry Centre, Chair of Analytical Chemistry, Institute of Chemistry, University of Rostock, 18059 Rostock, Germany
[c] Joint Mass Spectrometry Centre, Cooperation Group Comprehensive Molecular Analytics, Helmholtz Zentrum München-German Research Center of Environmental Health (GmbH), Ingolstädter Landstrasse 1, 85764 Neuherberg, Germany

ARTICLE INFO

Article history:
Received 23 July 2019
Revised 20 March 2020
Accepted 21 March 2020

Keywords:
Pyrolysis
Polyethylene terephthalate
REMPI
SPI
FT-ICR MS
APCI
TOF-MS

ABSTRACT

In the context of waste upgrading of polyethylene terephthalate (PET) by pyrolysis, this study presents three on-line mass spectrometric techniques with soft ionization for monitoring the emitted decomposition products and their thermal dependent evolution profiles. Pyrolysis experiments were performed using a thermogravimetric analyzer (TGA) under nitrogen atmosphere with a heating rate of 5 °C/min from 30 °C to 600 °C. Single-photon ionization (SPI at 118 nm/10.5 eV) and resonance enhanced multiple photon ionization (REMPI at 266 nm) were used with time-of-flight mass spectrometry (TOF-MS) for evolved gas analysis (TGA-SPI/REMPI-TOFMS). Additionally, the chemical signature of the pyrolysis products was investigated by atmospheric pressure chemical ionization (APCI) ultra high resolution Fourier Transform ion cyclotron resonance mass spectrometry (FT-ICR MS) which enables assignment of molecular sum formulas (TGA-APCI FT-ICR MS). Despite the soft ionization by SPI, the fragmentation of some compounds with the loss of the [O-CH = CH2] fragment is observed. The major compounds were acetaldehyde (*m*/*z* 44), benzoic acid (*m*/*z* 122) and a fragment of *m*/*z* 149. Using REMPI, aromatic species were selectively detected. Several series of pyrolysis products were observed in different temperature intervals, showing the presence of polycyclic aromatic hydrocarbons (PAHs), especially at high temperatures. FT-ICR MS data showed, that the CHO_4 class was the most abundant compound class with a relative abundance of 45.5%. The major compounds detected with this technique corresponded to *m*/*z* 193.0495 ($C_{10}H_9O_4^+$) and 149.0233 ($C_8H_5O_3^+$). Based on detailed chemical information, bulk reaction pathways are proposed, showing the formation of both cyclic monomer/dimer and linear structures.

1. Introduction

Pyrolysis is a versatile thermochemical technique that converts a solid material into useful gaseous, liquid, and solid products in absence of oxygen. This technique can be used to valorize various products, such as polymers, biomass, and tires. The material chosen in this study is polyethylene terephthalate (PET). PET is the third frequently consumed polymer in Europe after polypropylene and low density polyethylene (Kawecki et al., 2018). It is frequently used to make a variety of consumer goods, such as synthetic polyester fibers, bottles and films (Kawecki et al., 2018; Zander et al., 2018).

The pyrolysis of PET yields a complex mixture of products which consists of aldehydes (e.g., acetaldehyde, benzaldehyde), carbon oxides (CO_2 and CO), aliphatic hydrocarbons C_1-C_4 (e.g., CH_4, C_2H_4), aromatic species (e.g., benzene, toluene, styrene), carboxylic acids such as benzoic acid and its derivatives (e.g., acetylbenzoic acid, methylbenzoic acid, ethylbenzoic acid), terephthalic acid and vinyl terephthalate as well as esters (e.g., di-vinyl terephthalate, vinyl benzoate), ketones (e.g., acetophenone, benzophenone, fluorenone) and other compounds (Artetxe et al., 2010; Dzięcioł and Trzeszczyński, 2001; Dzięcioł and Trzeszczyński, 2000; Kumagai et al., 2017; Sophonrat et al., 2017; Yoshioka et al., 2004).

Different conventional methods were used in literature to characterize the pyrolysis products by online or offline analysis. Concerning offline analysis (i.e. after condensation), the most used

* Corresponding author.
E-mail address: valerie.vitzthum@univ-lorraine.fr (V. Burkle-Vitzthum).

https://doi.org/10.1016/j.wasman.2020.03.028
0956-053X/

analytical methods are Gas Chromatography coupled to Mass Spectrometry (GC-MS) and High Performance Liquid Chromatography (HPLC) (Çit et al., 2010; Dhahak et al., 2019). However, offline analysis does not allow the characterization of heavy species, which might be produced during the pyrolysis. For online analysis, PET pyrolysis experiments were mainly coupled to Fourier Transform Infrared Spectroscopy (FTIR), High Resolution Pyrolysis Gas-Chromatography and micro- GC (Badia et al., 2013; Czégény et al., 2012; Dhahak et al., 2019; Ohtani et al., 1986). These techniques are not able to analyze high mass compounds. Online analyses have the advantage of avoiding spurious reactions that can occur during the product condensation, and thus help predicting the genuine pyrolysis reaction pathways.

In the last decades, time of flight mass spectrometry (TOF-MS) has been widely applied (Lee et al., 2017; Shi et al., 2018; Wu et al., 2011). It provides high sensitivity and high acquisition speed (Green and Martin, 2006; Qian and Dechert, 2002). The identification of complex mixtures however often requires high resolution mass spectrometry which allows resolving multiple peaks with the same nominal m/z (Barrow et al., 2014). Fourier transform ion cyclotron resonance mass spectrometry (FT-ICR MS) has proven high potential for detecting and identifying compounds without pre-separation by chromatography (Bae et al., 2010; Kekäläinen et al., 2014). Molecular formula can be assigned to the resolved signals, typically within ppm mass accuracy (Huba et al., 2016).

Different ionization methods are available for mass spectrometry, all exhibiting different advantages and drawbacks. In fact, electron ionization (EI) in vacuum is the method commonly used for the evolved gas analysis of pyrolysis gases. It is a “hard” and universal ionization mode (Jia et al., 2016; Yuzawa et al., 2013). It leads to strong fragmentation of the molecule because of the high ionization energy generally deployed (70 eV) (Hsu and Ni, 2018). Consequently, the EI mass spectrum is complicated to interpret because of the absence of the molecular ions and strong overlapping signals of complex mixtures impeding data interpretation. In contrast, soft ionization techniques such as chemical ionization (CI), atmospheric pressure chemical ionization (APCI), electrospray ionization (ESI) or vaccum photo ionization (PI), a molecular ion (radical cation and/or protonated ion species) can be preserved and fragmentation is greatly diminished (Wang et al., 2015), although all to the latter methods are less universal than EI.

Photo ionization (PI) coupled to mass spectrometry has been widely used for the characterization of complex mixtures. PI can be divided in single-photon ionization (SPI) and resonance-enhanced multiphoton ionization (REMPI). SPI commonly involves a single-photon in the vacuum ultraviolet range (VUV) to ionize the molecule in one step, inducing little or no fragmentation (Giri et al., 2017; Hsu and Ni, 2018). The photon energy commonly used is between 7.5 and 11.8 eV, corresponding to a wavelength of 165–105 nm (Giri et al., 2017). In other words, only organic molecules with ionization energy lower than the photon energy can be ionized. Many types of lasers can be used to generate VUV light with different wavelengths such as Nd:YAG (118 nm; 10.48 eV (Rüger et al., 2018)), F_2 (157 nm; 7.9 eV (Trukhin and Golant, 2009)), H_2 (160 nm; 7.75 eV (Fukuzawa and Tanimizu, 1978)). Fig. 1 represents the ionization energies (IE) of compounds identified during PET pyrolysis (Sovová et al., 2008). IE are available from the

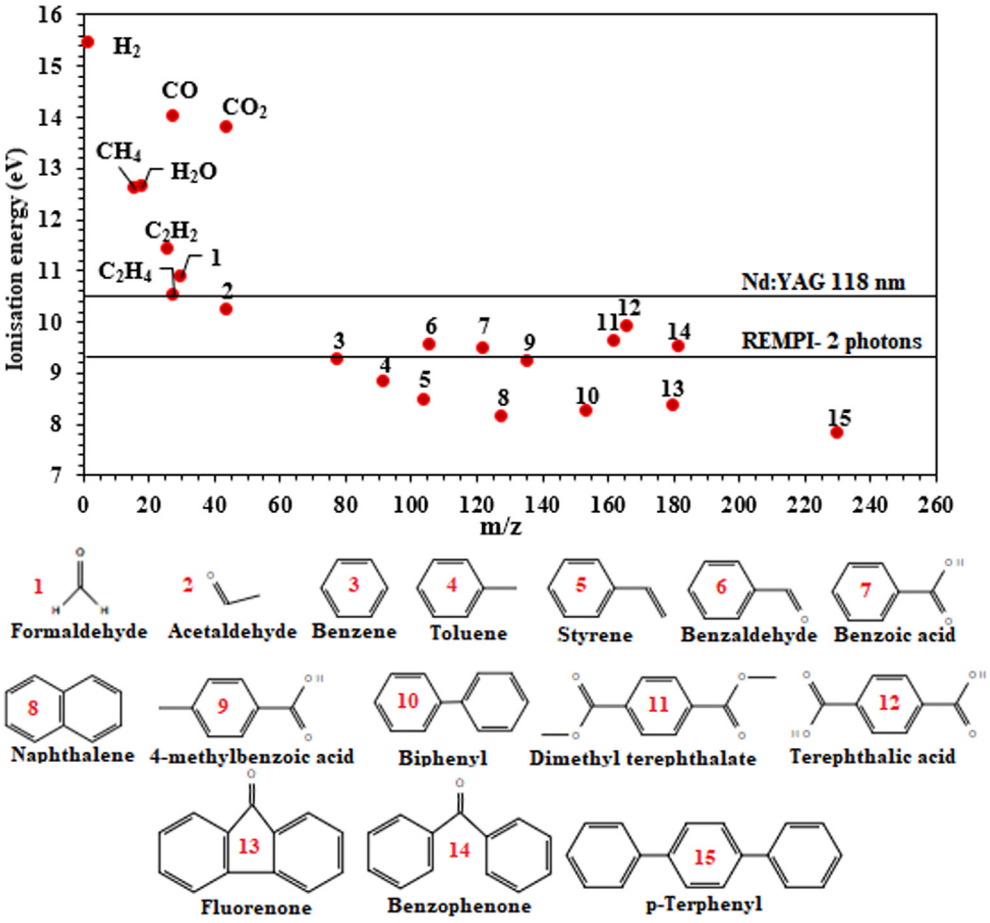

Fig. 1. Ionization energies of selected molecules identified in PET pyrolysis (adapted from refs (Hanley and Zimmermann, 2009; Jia et al., 2016)).

National Institute of Standards and Technology (NIST) (“NIST Chemistry webbook [Gas phase ion energetics data] Available online : https://webbook.nist.gov/chemistry/). IE of most compounds are below the photon energy, except certain small molecules, such as CO, CO_2, H_2O, H_2, and CH_4. Carbon oxides might represent a major proportion of PET pyrolysis gases, but cannot be ionized with common setups.

Unlike SPI, REMPI uses ultraviolet (UV) light, requiring at minimum two photons in which a single-photon or multiple photons absorbed excites an intermediate state and a second photon ionizes the atom or molecule (Jia et al., 2016). The soft ionization pathway, due to the low photon energies, leads to few fragmentation which facilitates the interpretation of the mass spectra. In addition, REMPI allows the selective detection of vibronic structure species such as mono- or polycyclic aromatic compounds and their derivatives (Dorfner et al., 2004; Zimmermann et al., 1999).

Another soft ionization technique commonly used, especially for FT-ICR MS, is atmospheric pressure chemical ionization (APCI) (Crepier et al., 2018). Corona discharge induced ion- molecule reactions in gas phase, generating radical cations or protonated molecule ions with little fragmentation (Li et al., 2015; Tose et al., 2015). This technique allows the detection of polar and medium polar compounds, preferably oxygenated species (Parr et al., 2018; Rüger et al., 2018). Due to instrumental limits of the FT–ICR MS, the mass range is between 100 and 1000. More details on the APCI process are given elsewhere (Li et al., 2015).

Numerous studies on pyrolysis have been performed by coupling thermogravimetry or pyrolysis experiments with the analytical techniques described above (Huang et al., 2017; Shi et al., 2018; Wu et al., 2011; Xu et al., 2017). These techniques provide not only the chemical formula of the analytes but also their evolution profile in real time. Consequently, temperature dependent pyrolysis products can be analyzed. So far, numerous studies focused on polymers such as polyethylene, polypropylene, polystyrene and polyvinyl chloride (Huang et al., 2017; Kai et al., 2019; Saraji-Bozorgzad et al., 2008; Wang et al., 2015; Wu et al., 2011; Zhou et al., 2019). However, limited studies have been conducted on oxygenated macromolecules such as polyethylene terephthalate (PET). Some PET pyrolysis experiments have been conducted on-line by using conventional analytical tools such as thermogravimetry (TGA) coupled to mass spectrometry (Gupta et al., 2004), TGA coupled to Fourier transform infrared spectroscopy (FTIR) (Badia et al., 2013; Czégény et al., 2012; Kinoshita et al., 1993; Pan et al., 2016), and Pyrolysis-gas chromatography (PyGC) (Ohtani et al., 1986).

In this study, three different analytical techniques were coupled to thermogravimetry for on-line monitoring of volatile compounds emitted by the slow pyrolysis of PET. Single-photon ionization (SPI) at 118 nm (10.5 eV) and resonance enhanced multi photon ionization (REMPI) at 266 nm were coupled to a time of flight mass spectrometer (TOF-MS). SPI is aiming at detection of organic species whose ionization energy are lower than 10.5 eV, whereas REMPI is suitable for the sensitive detection of aromatic and polyaromatic constituents. Another thermogravimetry analyzer was coupled to a Fourier transform ion cyclotron resonance mass spectrometer (FT-ICR MS) using atmospheric pressure chemical ionization (APCI). APCI FT-ICR MS is suitable to ionize medium-polar and polar species with a mass range [100–1000]. Using the FT-ICR MS exact mass data, detailed chemical information was gained and combined with the results obtained with SPI and REMPI. This procedure allowed for the detailed description of the pyrolysis process.

2. Materials and methods

2.1. Materials

PET was purchased from Goodfellow SARL (Lille, France) in a powder form (particle size of 300 μm). This polymer is amorphous with a crystallinity of 16%. The elemental analysis of carbon, hydrogen and oxygen content in PET was determined using a Flash Smart CHNS/O Analyser by Thermo Fisher Instrument. The oxygen content was calculated by difference. The results showed that PET contains about 45.5% carbon by mass, 36.4% hydrogen and 18.2% oxygen.

2.2. Instrumentation

2.2.1. Thermogravimetry coupled to SPI/REMPI-TOF-MS

A schematic overview of TG-REMPI/SPI-TOF-MS is presented in Fig. 2a) (Rüger et al., 2018). The thermobalance (STA 409, Netzsch Geratebau, Selb, Germany) was on-line coupled to the ionization source of the mass spectrometer using a heated transfer line (280 °C, ID 280 μm × 2.25 m length). 8–10 mg of PET was filled in an aluminum oxide crucible and heated up to 550 °C with a constant heating rate of 5 °C/min. The nitrogen flow rate around the sample was fixed to 50 mL/min for reactive gas and 50 mL/min for protective gas.

The ionization source was operated under vacuum conditions (around 10^{-4} mbar) which allows transferring an aliquot fraction of evolved gas out of the thermobalance inside the mass spectrometer based on the pressure gradient. A Nd:YAG laser (Surelite III, Continuum, Inc., Santa Clara, CA, U.S.A; wavelength: 1064 nm (Czech et al., 2016)) was used in this experiment. A beam at 355 nm was produced by frequency tripling conversion. It operated with pulse energies of 25 mJ, pulse width of 5 ns, and repetition

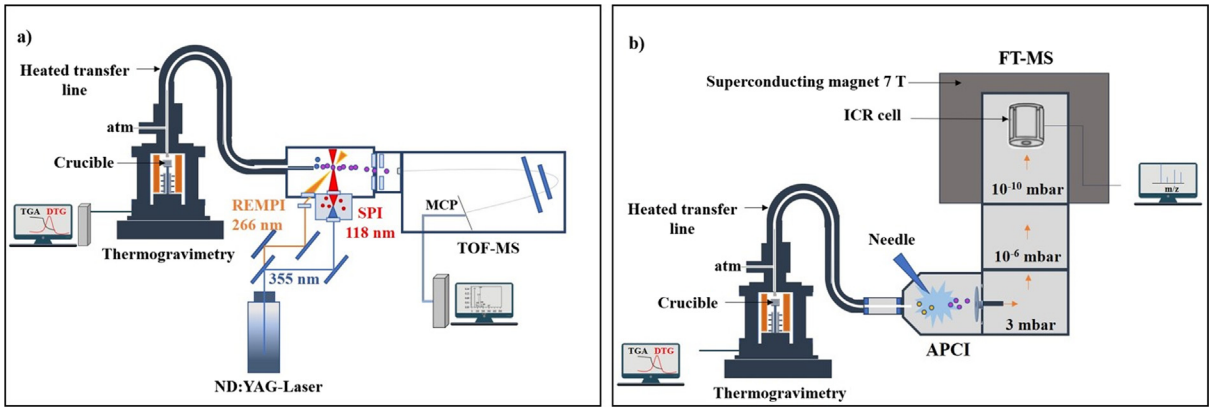

Fig. 2. Schematic of the instrumental setup of: (a) TGA-REMPI/SPI-TOF-MS; (b) TGA-APCI FT-ICR MS (adapted from refs (Rüger et al., 2018; Rüger et al., 2015).

rate of 10 Hz. For SPI, the wavelength was again tripled, generating a vacuum ultraviolet light (118 nm, 10.5 eV), by using a xenon-filled gas cell (Xe 4.0, 12 mbar). For REMPI, a wavelength of 266 nm (4.66 eV) was obtained by frequency-quadrupling of the Nd:YAG laser 1064 nm. Consequently, the energy ionization with REMPI using two photons is 9.32 eV. Further details are available elsewhere (Czech et al., 2016; Fendt et al., 2013).

Once the ions are generated, they are *m*/*z*-separated using a reflectron TOF analyzer (Kaesdorf Instrumente für Forschung and Industrie, Munich, Germany) and detected by a microchannel plate (MCP, Chevron Plate, Burle Electro-Optics Inc.) (Czech et al., 2016; Rüger et al., 2018). The ions were recorded up to *m*/*z* 500. A custom LabView-software was used for data processing (Czech et al., 2016).

2.2.2. Thermogravimetry coupled to APCI/FT-ICR-MS

A thermobalance (STA 209, Netzsch Gerätebau GmbH, Germany) was used for pyrolysis experiments (Fig. 2b). A mass of 1–1.5 mg sample was loaded in an aluminum crucible and heated under a constant nitrogen flow of 200 mL/min from 20 °C to 600 °C with a heating rate of 5 °C/min. Approximately 2 mL/min of the evolved gas mixture was transferred to the ionization chamber via a slight overpressure of 5 mbar by a heated transfer line (deactivated fused silica capillary, 2 m, 0.53 mm ID, 300 °C). The chemical ionization was carried out by a modified Bruker GC-APCI II source, operating at atmospheric pressure in positive ion mode. For ionization, a stainless-steel needle was used, generating a corona discharge with a current of 2.5 μA. More details have been given elsewhere (Rüger et al., 2015). The ions produced were detected by a Bruker Apex II ultra FT–MS equipped with a 7T magnet (InfinityCell, Bruker Daltonics, Bremen, Germany). A mass range of 100–1000 was recorded with five microscans per spectrum. A 4 Megaword transient of approximately 2 s length was applied, offering an ultrahigh resolution of 260,000 at *m*/*z* 400 was obtained.

Data processing was carried out using Bruker DataAnalysis for *m*/*z*-calibration of the spectra and a self-written tool CERES based on Matlab scripting for further processing and sum formula calculation. Every measurement was internal linearly calibrated in DataAnalysis and again every single spectrum during processing in CERES. For sum formula assignment, the following restrictions were applied: $C_{4-100}H_{4-200}N_0O_{15}S_0$, H/C ratio of 0–3 and Double Bond Equivalent (DBE) of 0–40.

3. Results and discussion

3.1. Evolved gas analysis by Single-photon ionization (SPI) mass spectrometry

Fig. 3a) shows the residual mass (TGA), the derivative of the mass loss signal (DTG) and the total ion current (TIC) as a function of temperature. Over the whole pyrolysis time, the TIC is obtained by adding all ions of the spectra obtained at a defined time. Visibly, the evolution of TIC coincides with the DTG curve. This indicates that SPI detected some of the major volatile degradation products of the PET pyrolysis, excluding CO_2 and CO. The decomposition starts at roughly 350 °C and lasts approximately up to 500 °C. The maximum of TIC and DTG corresponds to 435 ± 1 °C.

Fig. 3b) displays the average mass spectra for selected temperature ranges of the emitted compounds. The structure of the molecules was determined based on literature (Guo et al., 2015) (Sovová et al., 2008). It should be noted that the temperature indicates the evaporation of molecules and they can be generated before in the condensed phase. Signal intensities increase steadily up to a temperature of 450 °C. In the 350–400 °C temperature range, major degradation products appear, and their intensities increase as the pyrolysis temperature increases. Signals at *m*/*z* 44, 122, and 166 most likely correspond to acetaldehyde, benzoic acid, and terephthalic acid, respectively. Based on the literature, the peak corresponding to *m*/*z* 149 is a characteristic fragment of vinyl terephthalate (M_w = 192 g/mol) which is reported to be one of the primary compounds of PET degradation (Garozzo et al., 1987; Plage and Schulten, 1990). Thus, a mass loss of *m*/*z* 43 occurs, which can be attributed to a [O-CH=CH_2] fragment (Garozzo et al., 1987; Plage and Schulten, 1990). Despite soft ionization, the carbon - carbon double bond (C=C) is destabilized followed by the oxygen ester, undergoing photo-fragmentation under these conditions (Van Dam and Oskam, 1978). An example in the literature of photoionization of vinyl butyrate which has the same fragment in its structure proved that the fragmentation occurs from 9.5 eV by losing *m*/*z* 43 (Czekner et al., 2018). Losing the same group, the peaks at *m*/*z* 105 and 175 may also be the results of fragmentation of vinyl benzoate (M_w = 148 g/mol) and di-vinyl terephthalate (M_w = 218 g/mol), respectively. On the other hand, the intensities of major products reach a maximum between 400 °C and 450 °C and decrease there after which shows either the end of the pyrolysis or the presence of secondary reactions causing their intensities diminution. The intensity of terephthalic acid (*m*/*z* 166) decreases slightly between 450 and 500 °C, even so it becomes the compound with the highest intensity at high temperatures, as shown in Fig. 3b).

Possible peak assignments of major compounds are summarized in Table S1. The mixture mostly contains acids and vinyl end groups. The same observation was made by (Garozzo et al., 1987) using electron ionization at low electron energy (18 eV) for copolyesters containing ethylene terephthalate and p-oxybenzoate units. They studied the on-line pyrolysis coupled to mass spectrometry with a heating rate of 10 °C/min. (Garozzo et al., 1987) observed the loss of 43 [O—CH=CH_2] and 17 [OH] mass units, confirming the metastable transitions of fragments and indicating the presence of open chain structures with carboxyl and vinyl end groups. Each compound corresponding to a specific *m*/*z* can be easily real-time-monitored. The thermal evolution profiles of major *m*/*z* are plotted in Fig. 3c). Acetaldehyde (*m*/*z* 44) is the first compound detected by TOF-MS, at about 315 °C, followed by benzoic acid (*m*/*z* 122) at 350 °C. The terephthalic acid (*m*/*z* 166) is detected at 371 °C, 21 °C after the detection of benzoic acid and 7 °C after benzene (*m*/*z* 78). The maximum productions of major compounds are observed at 431 °C, except for terephthalic acid (*m*/*z* 166) which is observed at 440 °C. Interestingly, the benzene curve shows a bi-modal emission behaviour in which the maximum of the first peak is detected at 427 °C and the second maximum at 470 °C. Benzene goes through a minimum at 447 °C. The same trend was observed in (Dhahak et al., 2019) using a horizontal reactor. In this study, online monitoring of gases (carbon oxides, ethylene and benzene) during slow pyrolysis (5 °C / min) was performed. Benzene profile also showed two peaks at 431 °C and 469 °C. The first and the second peaks may be due to the decarboxylation of benzoic acid and terephthalic acid, respectively. The production of benzene is accelerated at higher temperature, as shown in Fig. 3c).

3.2. Evolved gas analysis by Resonance-enhanced multiphoton ionization (REMPI) mass spectrometry

Using REMPI, only aromatic species can be detected. However, aromatic carboxylic acids such as terephthalic acid and benzoic acid cannot be ionized because of their high ionization energy (Fig. 1). Benzene, which has a ionization energy of 9.24 eV, also requires a little more energy to be ionized (≥9.5 eV) (Boesl et al., 1978). Fig. 4a) shows the TIC and DTG curves. Contrary to the SPI-TIC, REMPI-TIC exhibits a bi-modal behavior as the tempera-

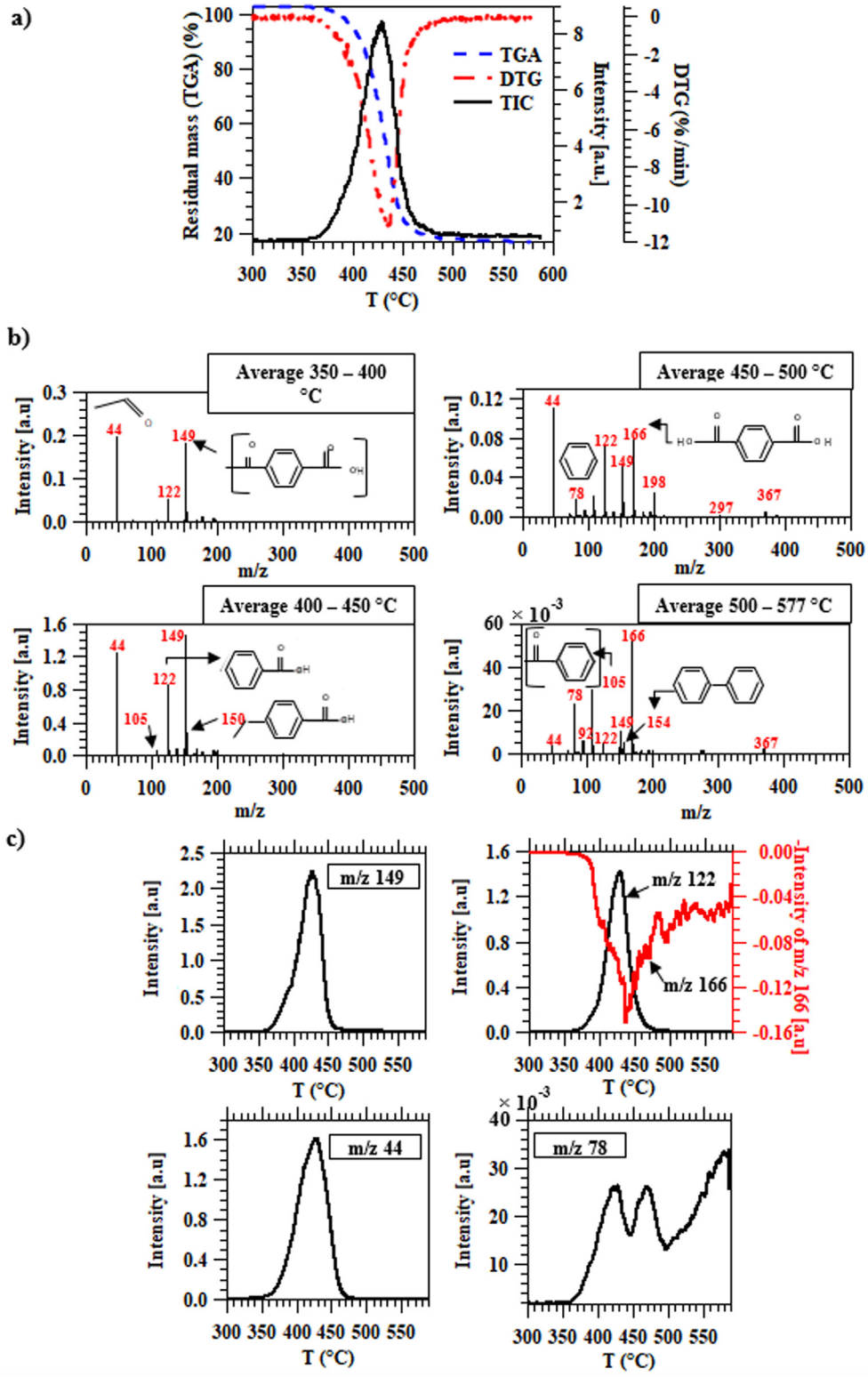

Fig. 3. TGA-SPI TOF-MS results: (a) TGA, DTG, TIC curves, (b) Average mass spectra of the products at various temperatures, (c) thermal evolution profiles of major *m*/*z*.

ture increases. The first peak coincides with the DTG curve, whereas the second peak appears in a region where the mass loss is almost finished, indicating the presence of secondary reactions with a small mass loss. The maximum peaks correspond to 435 °C and 473 °C, respectively. These two peaks highlight the presence of two different mechanisms responsible for the formation of aromatic species such as polycyclic aromatic hydrocarbons (PAHs). REMPI mass spectra are shown in Fig. S1. For both peaks observed in the REMPI-TIC curve, an average mass spectrum is presented in Fig. S2. The mass spectrometric pattern is significantly different when comparing the two stages, and they depend mainly on temperature. The effect of temperature on the pyrolysis product intensities is depicted in Fig. 4b). As can be seen, a higher variety of compounds is detected in REMPI than in SPI. Different series of

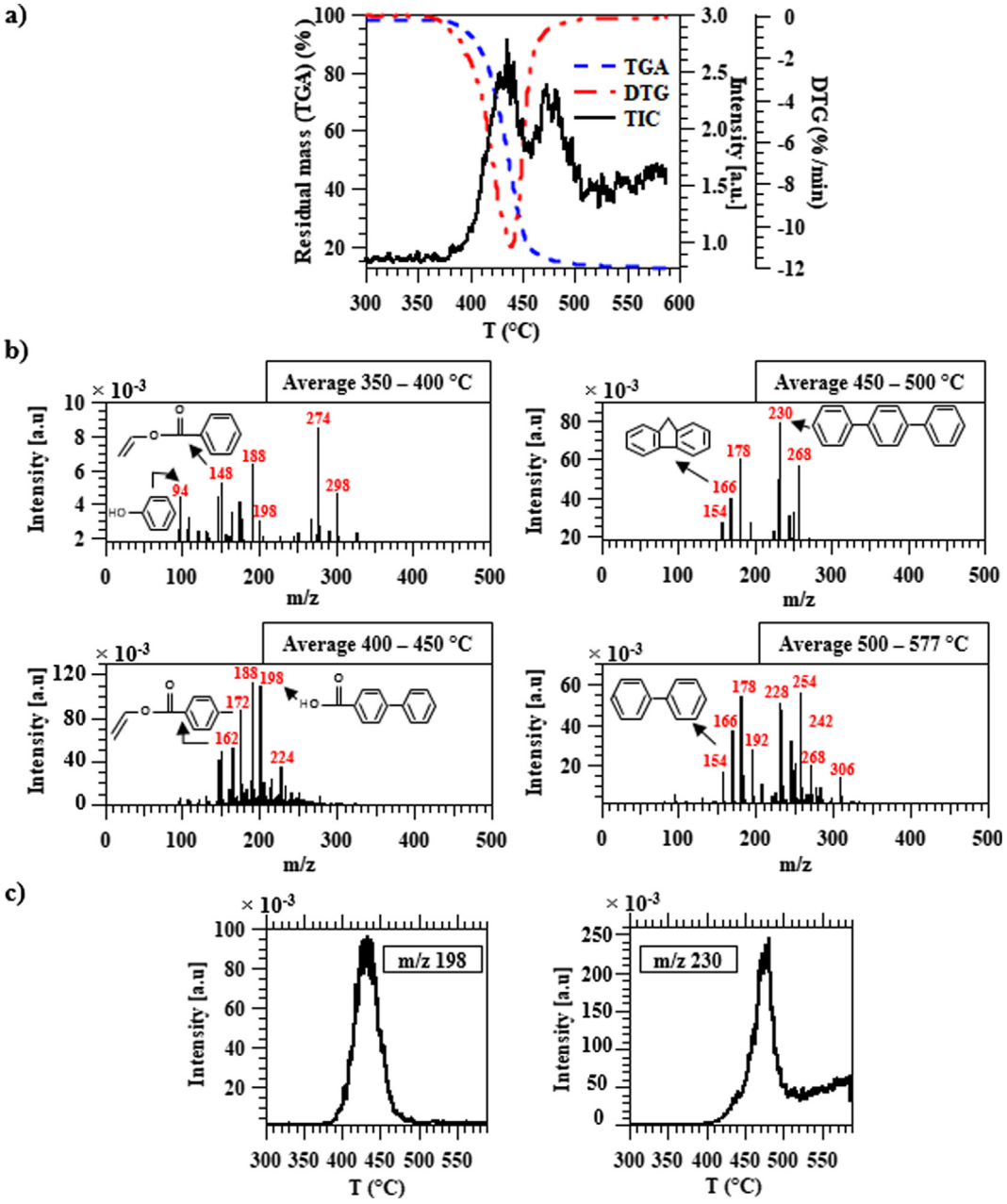

Fig. 4. TGA-REMPI TOF-MS results: (a) TGA, DTG, TIC curves, (b) Average mass spectra of the products at various temperatures, (c) thermal evolution profiles of major *m*/*z*.

pyrolysis products are observed at different temperature intervals. This evolved gas complexity confirms the presence of different and various reactions involved in the pyrolysis of PET. In fact, between 300 °C and 350 °C, *m*/*z* of 274, 298, 264, and 288 are detected with low average intensities. With the increase of temperature, the mass spectrum shows other peaks such as *m*/*z* of 192, 188, 148, 144, 94, and 162. The *m*/*z* of 148, 94, and 162 presumably correspond to vinyl terephthalate, vinyl benzoate, phenol, and vinyl 4-methylbenzoate, respectively. Using REMPI, compounds with [O—CH=CH_2] do not undergo a photo-fragmentation, because of the low energy. However, their sensitivity of detection by REMPI is much lower than by SPI.

The signal intensities of aromatic products increase at higher temperatures. The highest intensities are observed between 400 °C and 450 °C, which corresponds to the maximum decomposition rate of PET. In this phase, the major compounds correspond to *m*/*z* of 188, 198, 172, and 162. At higher temperature (450–577 °C), other compounds appear such as *m*/*z* 254, 228, 178, 230, 166, and 154. Based on literature (Hujuri et al., 2013; Sovová et al., 2008), those peaks may be attributed to 1,2′-binaphthalene, benzo[a]anthracene, anthracene or/and phenanthrene, terphenyl, 9H-fluorene and biphenyl or/and acenaphthene, respectively (Table S1). The presence of PAHs is mainly detected between 450 and 500 °C, confirming the presence of secondary reactions and most likely causing the second peak in REMPI-TIC.

The evolution profile of major peaks is shown in Fig. 4c). The maximum productions of the different aromatics do not occur at the same time. Terphenyl, which corresponds to *m*/*z* 230, approximately appears at 415 °C and reaches a maximum at 477 °C. The peak at *m*/*z* 198, which may probably correspond to biphenyl-4-carboxylic acid ($C_{13}H_{10}O_2$) (Deng et al., 2006; Guo et al., 2015; Sovová et al., 2008), evolves starting from 389 °C to 492 °C. Its maximum production occurs at 439 °C. The evolution profile of *m*/*z* 198 detected by REMPI resembles to the SPI signals (Fig. S3).

3.3. Evolved gas analysis by TGA-APCI FT-ICR MS

The DTG, TIC, and temperature curves revealed by thermogravimetric coupling to APCI FT-ICR MS are shown in Fig. S4. The temporal evolution of the decomposition rate (DTG) is consistent with the TIC curve, showing a single peak. A similar trend was observed by SPI-TOF-MS (Section 3.1). The maximum decomposition rate is found at about 417 °C. Typical diagrams are constructed to facilitate the visualization and interpretation of high-resolution mass spectrometric data, such as double bond equivalence (DBE) against carbon number and Van-Kreleven plot. DBE is a measure of unsaturation (double bonds and rings) in a molecule and contributes to the prediction of the chemical structure from a given elemental formula. Besides, Van-Krevelen diagram is a graphical distribution of H/C ratio versus O/C, providing an overall view on compound categories (Miettinen et al., 2017; Oni et al., 2015). The evolution of double bond equivalence (DBE) versus carbon number is shown in Fig. 5.a). It indicates that there are compounds with DBE values ranging from 2 to 15 and carbon numbers ranging from C_6 to C_{20}. The high DBE values confirm the presence of polycyclic aromatic hydrocarbons. Most of the detected compounds have a relatively low abundance (in blue color). The highest abundances (red color) correspond to species with a carbon number C_8-C_{10} and a DBE of 6–7. The core structure of these compounds is probably based on one benzene ring (DBE of 4) or two aromatic rings (DBE of 7). Fig. 5.b) represents the Van-Krevelen plot, highlighting different compound classes. For instance, a complex mixture of aromatic compounds with expanded oxygen content is mainly distributed within a H/C range of 0.7–1 and O/C values in the range of 0.1–0.5, as well as highly unsaturated compounds (H/C $\leq$1.5) and little aliphatic compounds (1.5 $\leq$ H/C $\leq$ 2) (Li et al., 2018). Furthermore, polycyclic and aromatic compounds without oxygen are also present with H/C $\approx$ 0.5–1 and account for roughly 6.4% of the overall signal. The class distribution of detected species is shown in Fig. 5c). Seven classes are observed

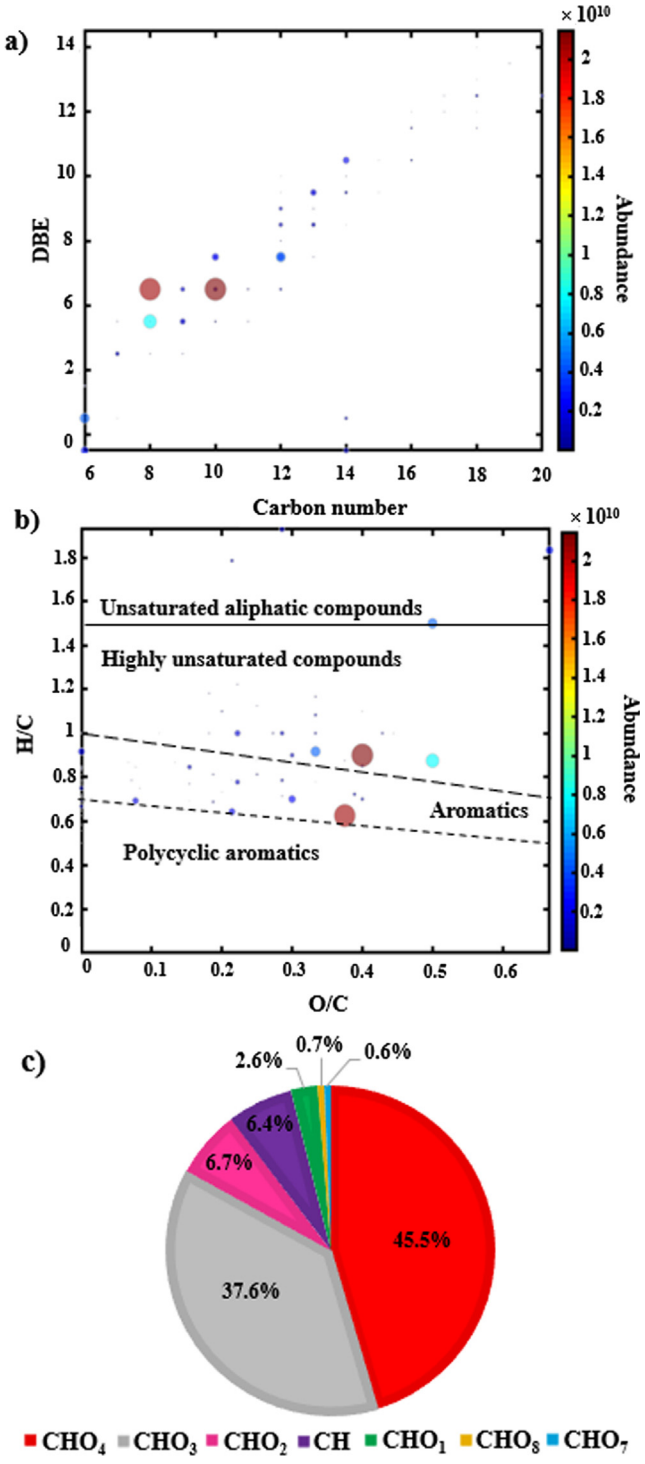

Fig. 5. TGA-APCI FT-ICR MS results: (a) Double bond equivalent (DBE) vs carbon number plot, b) Van Krevelen plot (H/C vs O/C), (c) Pie chart representing the compound class distribution. In (a) and (b), the size of the dots is proportional to the abundance.

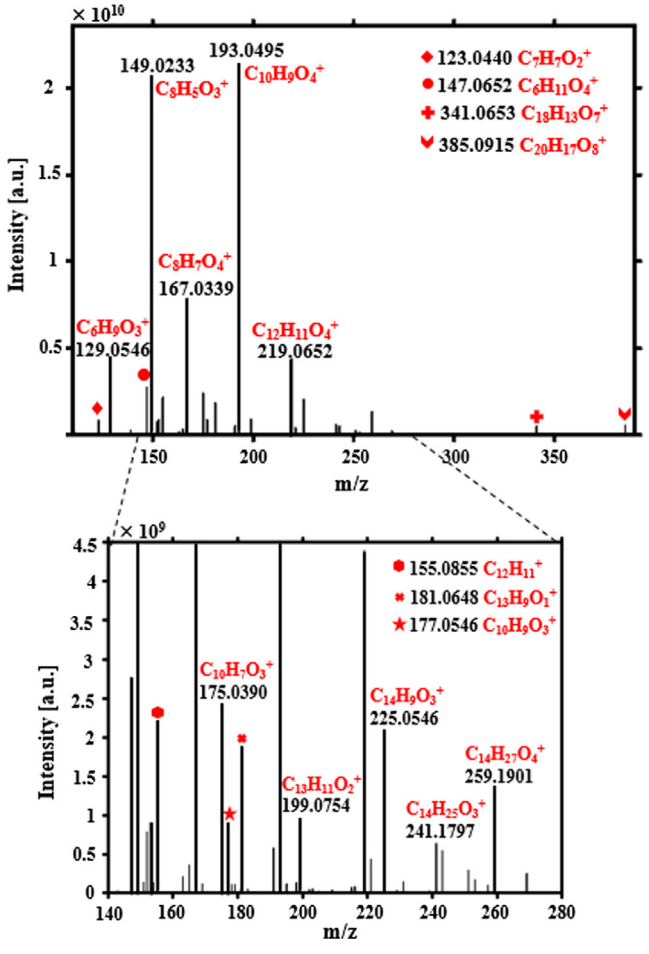

Fig. 6. Average APCI FT-ICR MS spectrum of pyrolysis products of PET.

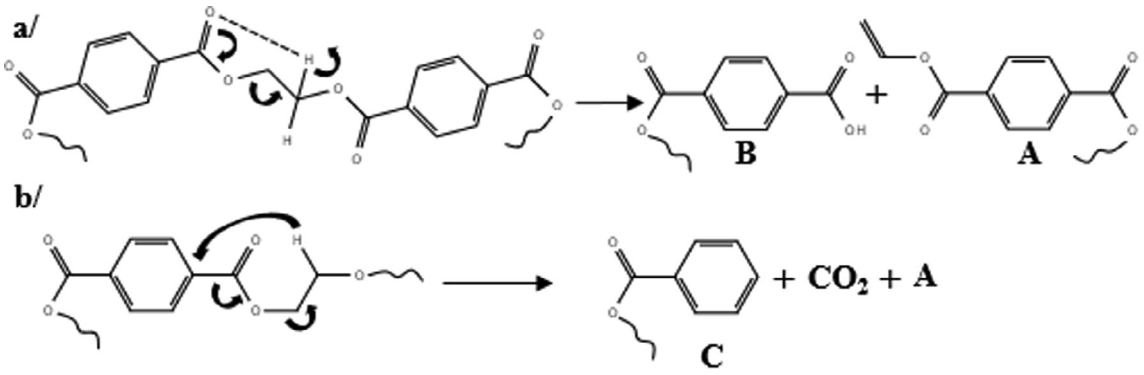

Fig. 7. Intramolecular possibilities in PET degradation.

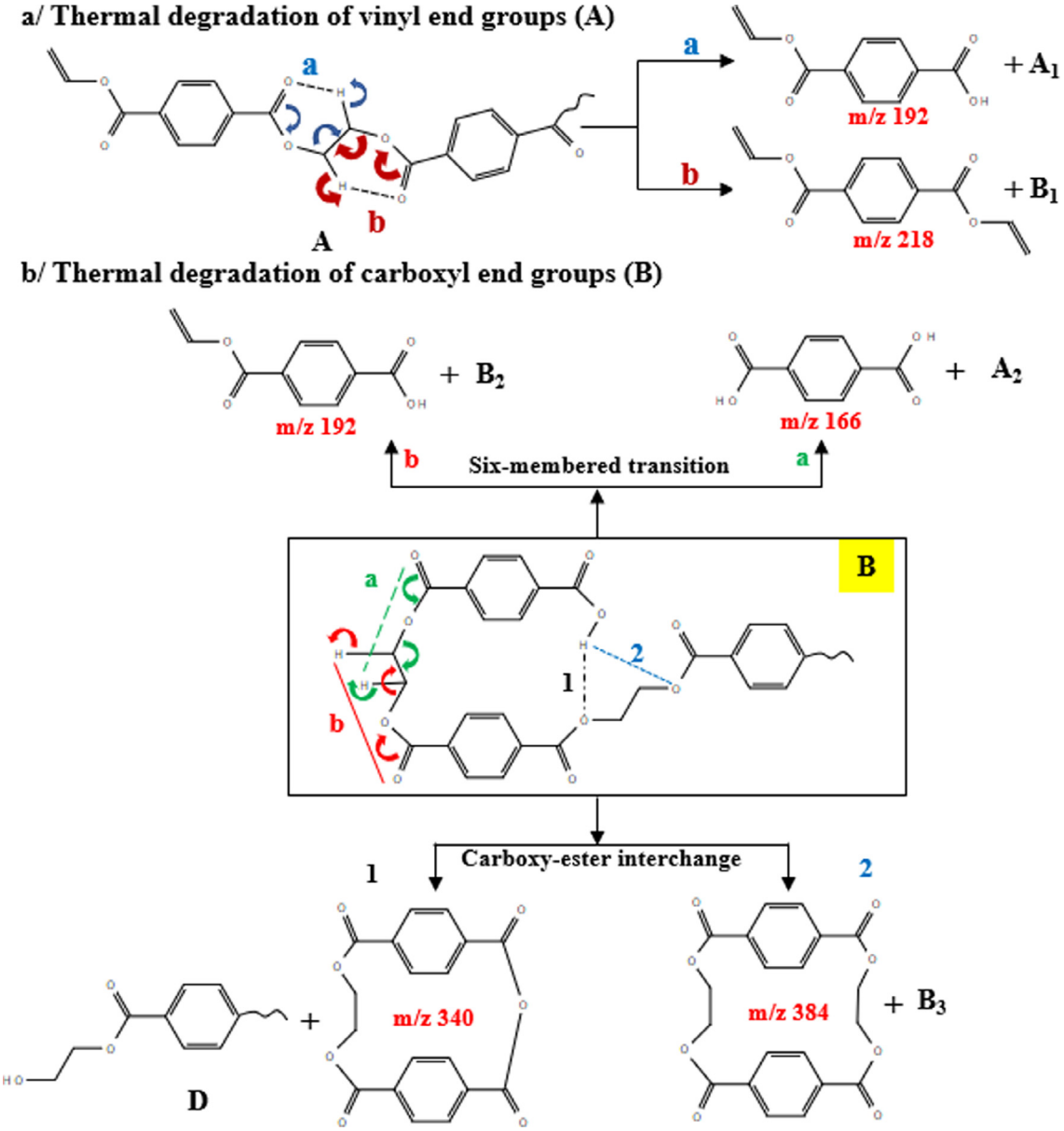

Fig. 8. Proposed reaction pathways for the degradation of: a/ vinyl end groups, b/ carboxyl end groups.

in APCI FT-ICR MS in which the oxygenated category CHO_x is the prevailing class. The most abundant CHO_x compounds are those containing 4 and 3 oxygen atoms with a percentage of 45.5% and 37.6% respectively. Very low abundances of highly oxygenated compounds (7 and 8) (<1%) are also detected.

An APCI FT-ICR mass spectrum is shown in Fig. 6. A unique molecular formula is attributed to each peak detected using the accurate mass measurement.

The species are detected mainly as protonated molecule $[M+H]^+$ and to a part as molecular cation $[M]^+$, where M refers to the molecule. Seventy-seven peaks are assigned unambiguously in the 100–400 *m/z* range. Possible peak assignments of major compounds are summarized in Table S1. The highest intensities are observed at *m/z* 193.0495 and 149.0233, corresponding to $C_{10}H_9O_4^+$ and $C_8H_5O_3^+$ respectively. The peak at *m/z* 385.0915 ($C_{20}H_{17}O_8^+$) is the highest mass obtained by FT-ICR-MS and may be attributed to cyclic or/and linear dimer (Nasser et al., 2005). (Ubeda et al., 2018) reported similar results. In their study, they analyzed the oligomer of PET by using ultra-high-performance liquid chromatography-quadrupole time-of-flight mass spectrometry (UPLC-MS-QTOF). They found that the cyclic monomer and dimer are characterized by an exact *m/z* of 193.0498 and 385.0915, respectively. Signals corresponding to *m/z* 219.0652 ($C_{12}H_{11}O_4^+$) and *m/z* 167.0339 ($C_8H_7O_4^+$) can be attributed to divinyl terephthalate and terephthalic acid, respectively. The temporal evolution profiles of the compounds with the highest intensities are shown in Fig. S5. Peaks at *m/z* 193.0495 ($C_{10}H_9O_4^+$) and 149.0233 ($C_8H_5O_3^+$) are detected by FT-ICR MS at the same temperature, about 346 °C. Terephthalic acid (*m/z* 167.0339 ($C_8H_7O_4^+$)) is detected at 361 °C. A cyclic dimer (*m/z* 385.0915 ($C_{20}H_{17}O_8^+$)) and an anhydride compound at *m/z* 341.0653 ($C_{18}H_{13}O_7^+$) appear later at 381 °C (Fig. S6). These compounds are among the primary

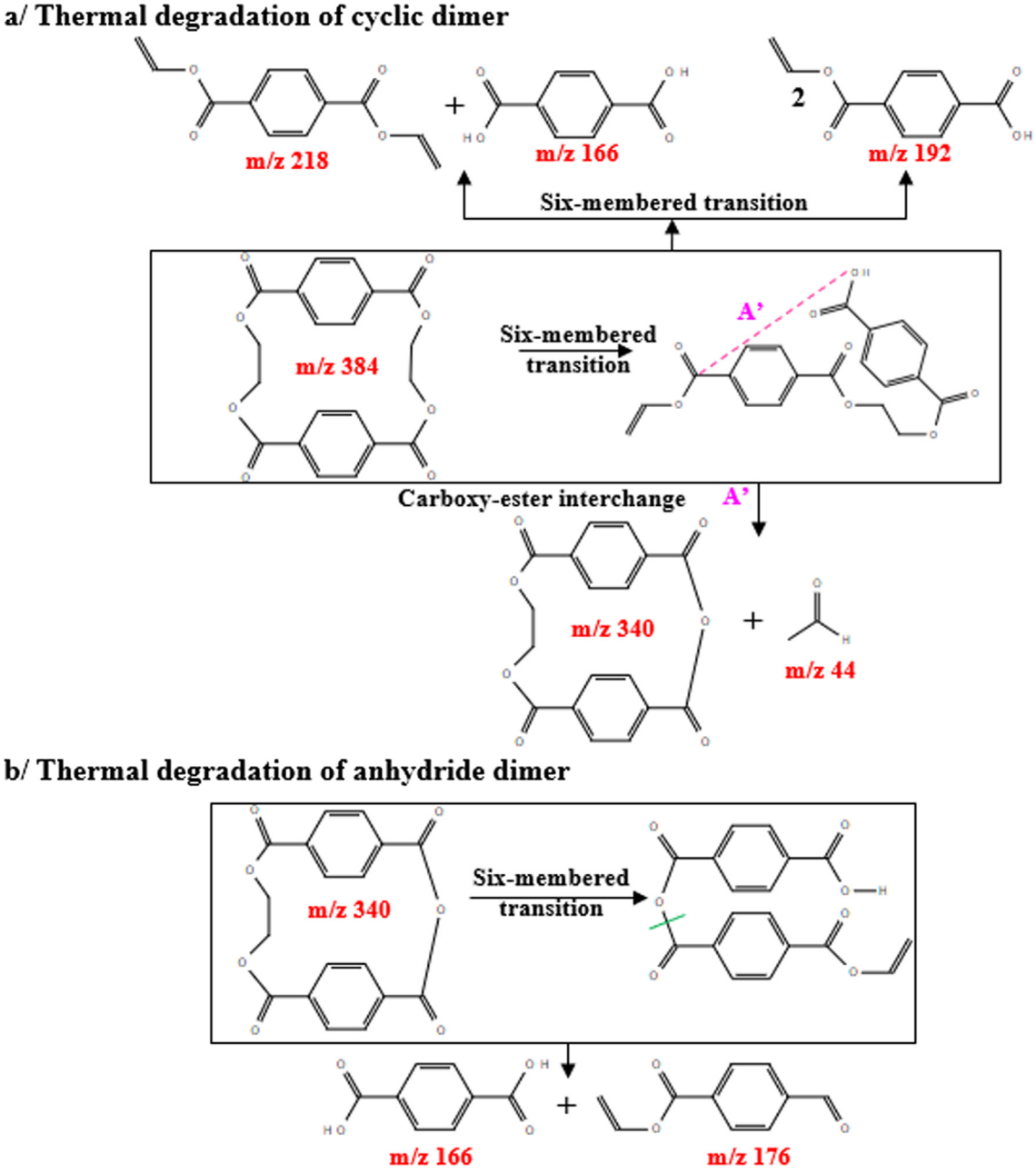

Fig. 9. Proposed reaction pathways for the degradation of: a/cyclic dimer, b/ cyclic anhydride.

products of the degradation of PET, and their delayed detection may indicate that they are generated in condensed phase (solid or liquid) and transferred into the gas phase at higher temperatures.

In the literature, (Dhahak et al., 2020) characterized molecules formed during PET pyrolysis and analyzed offline by Fourier Transform Ion Cyclotron Resonance Mass Spectrometry (FT ICR–MS) coupled to electrospray (ESI). Some molecules such as *m*/*z* 358 and *m*/*z* 550 that had been detected by ESI-FT-ICRMS are not observed in the present study and this seems to indicate that these molecules may be formed by repolymerization in the condensers or in the cold zone. This highlights the strength of online analysis versus offline analysis.

3.4. Possible reaction pathways for PET degradation

Different reaction pathways for PET degradation can be proposed, involving most likely two back-biting possibilities through a concerted mechanism (Fig. 7). Reaction in Fig. 7a) is more energetically favorable than the reaction in Fig. 7b), involving the six-membered cyclic transition state, as reported in previous studies (Hujuri et al., 2013; Montaudo et al., 1993; Plage and Schulten, 1990). The transition state energy of dissociation is about 50 kcal/mol (Dayma et al., 2019). It leads to the formation of carboxyl and vinyl end groups. In the second possibility, PET may undergo a decarboxylation reaction, producing benzene and vinyl

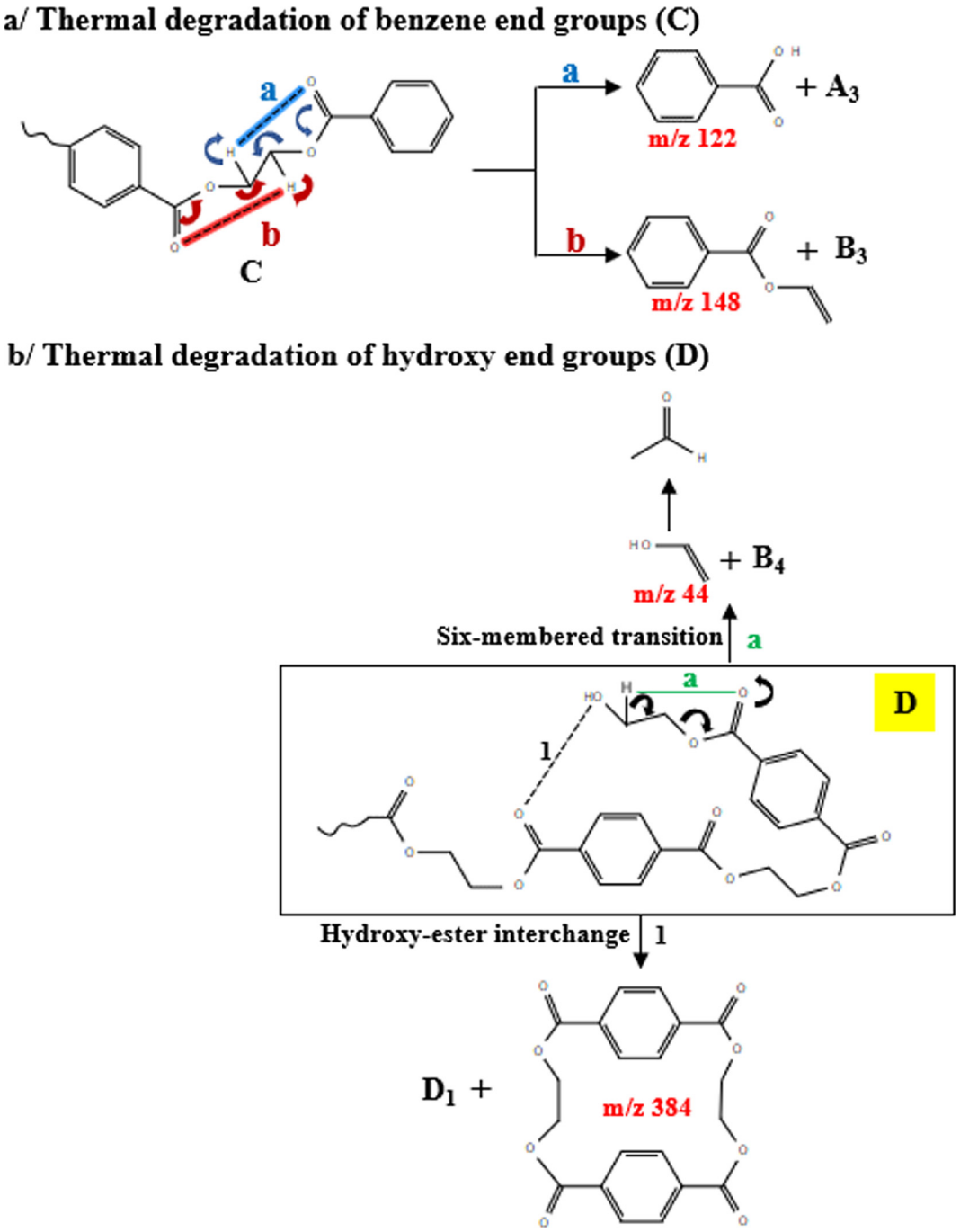

Fig. 10. Proposed reaction pathways for the degradation of: a/benzene end groups, b/ hydroxyl end groups.

end groups. Vinyl decompose via six-membered cyclic transition state, as shown in Fig. 8a), producing di-vinyl terephthalate (*m*/*z* 218), vinyl terephthalate (*m*/*z* 192), as expected (Hujuri et al., 2013), and other carboxyl and vinyl end groups, having lower molecular weights. Carboxyl end groups may undergo two different reactions Fig. 8b). In fact, a six-membered cyclic transition state which generates terephthalic acid (*m*/*z* 166), vinyl terephthalate (*m*/*z* 192), and carboxyl and vinyl end groups, according to two different branches in the same molecule.

Additionally, an intramolecular carboxy-ester interchange may take place, leading to the formation of cyclic products, such as cyclic dimer (*m*/*z* 384), hydroxy and carboxy end groups. (Montaudo et al., 1993) investigated the direct pyrolysis of PET using negative chemical ionization. They found that cyclic oligomers are the primary products at about 300 °C that decompose further by β-H transfer reactions at 400 °C generating open-chain oligomers with olefin and carboxylic end groups.

(Samperi et al., 2004) also studied the isothermal degradation of PET in the temperature range of 270–370 °C using matrix-assisted laser desorption ionization–time of flight (MALDI-TOF) mass spectrometry and NMR analysis. They indicated the formation of cyclic oligomers, and proposed their structural characterization. Anhydrides containing oligomer may also be generated at *m*/*z* 340, which is in agreement with literature (Samperi et al., 2004).

Possible reaction pathways for the degradation of cyclic dimer and anhydrides are shown in Fig. 9. Six-membered transition state occurs to generate linear dimer and anhydride. These linear dimers may undergo carboxy-ester interchange producing cyclic anhydrides and acetaldehyde. Fig. 10.a) shows that benzoic acid (*m*/*z* 122), vinyl benzoate (*m*/*z* 148) and carboxyl and vinyl end groups can be generated via the six-membered transition in benzene end groups (**C**).

In the case of hydroxy end groups, an intramolecular hydroxy-ester interchange, as shown in Fig. 10b), may occur and produces cyclic dimer (Murillo et al., 2010). In literature, the presence of hydroxy end in the structure accelerates the interchange reaction and favored the formation of cyclic products (Chikh et al., 2003; Kamoun et al., 2006). Vinyl alcohol (*m*/*z* 44) is also generated via six-membered transition, however, it transforms to acetaldehyde, which is one of primary volatile products in PET degradation (Fig. 10b). Among the volatile PET degradation species are ethylene (C_2H_4), which is formed with a smaller extent. An intermolecular reaction through an eight-membered transition between PET and vinyl end groups is proposed for its formation (Fig. 11) (Levchik and Weil, 2004).

In addition, tentative degradation pathways of major products are illustrated in Fig. 12. The routes proposed here are consistent with the main products identified by the three techniques. The starting point is the di-vinyl terephthalate (*m*/*z* 218). In literature, Taylor reported various reactions occurred in vinyl acetate decomposition between 363 and 448 °C (Taylor, 1983). By analogy, every compounds with a [(C=O)O(CH=CH_2)] segment undergoes the same routes.

Traces of acetylene (C_2H_2) also exists in PET degradation (Sovová et al., 2008; Turnbull et al., 2013). Unfortunately, it cannot be detected with the three techniques because of its high ionization energy and lower molecular weight. The formation of acetylene may be the by-product of vinyl end groups degradation.

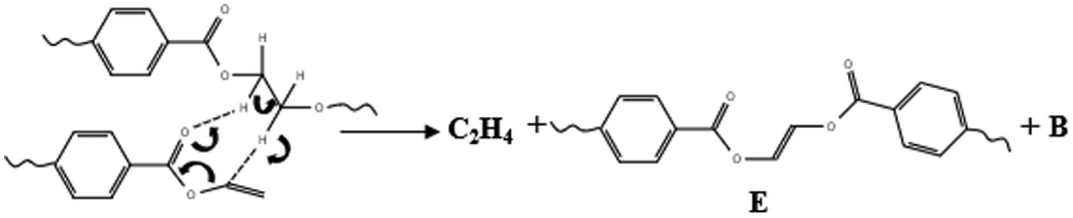

Fig. 11. Formation of ethylene.

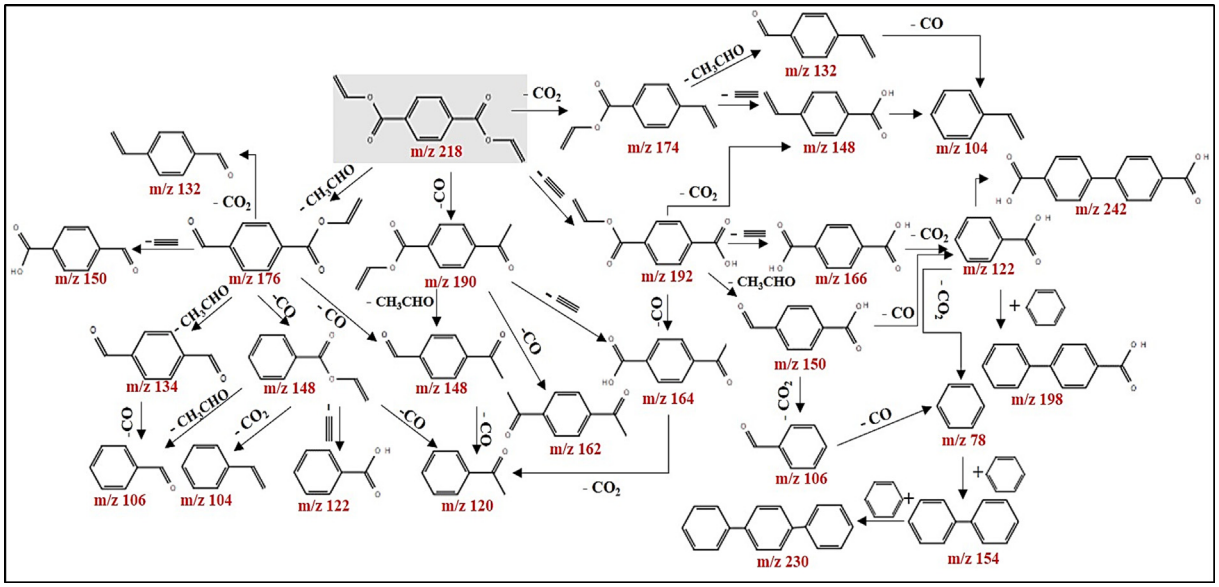

Fig. 12. Proposed reaction pathways for the degradation of major products.

Polycyclic aromatic hydrocarbons (PAHs), such as biphenyl (*m*/*z* 154) and terphenyl (*m*/*z* 230), are also presented. They are most likely produced via benzene.

4. Conclusion

In this study, three different soft ionization mass spectrometric approaches have been applied, allowing a comprehensive overview and understanding of the slow pyrolysis of PET in real time. The originality of this paper firstly lies in on-line monitoring of the emitted decomposition products and their thermal dependent evolution profiles. Secondly, the combination of these techniques allows the almost complete identification of volatile species and therefore, the typical reactions that can occur. TG-SPI-TOF-MS was used for the description of organic species with ionization energies below 10.5 eV. This technique showed that the main major peaks were acetaldehyde (*m*/*z* 44), benzoic acid (*m*/*z* 122) and a peak at *m*/*z* 149 which is a fragment of the monomer of PET (*m*/*z* 192). Despite the use of soft ionization, some compounds fragmented with the loss of a [O—CH=CH_2] fragment. Aromatic compounds, such as benzene and toluene, exhibited a bi-modal behavior in their profiles showing the existence of two different reactions involved in their formation. The second soft ionization technique used was REMPI-TOF-MS, selective for aromatic species. REMPI-TIC has the same trend as the benzene profile. Different series of pyrolysis products are observed in different temperature intervals. The main products correspond to *m*/*z* 230, 178, and 254. Possible structures were proposed in SPI and REMPI techniques. Additionally, FT-ICR MS was applied, detecting medium-polar and polar species in a mass range of [100–40]. Compounds with DBE values ranging from 2 to 15 and carbon numbers ranging from C_6 to C_{20} were detected. Seven classes were observed in which the most abundant was CHO_4, with a percentage of 45.5%. Detailed chemical information was gained using FT-ICR exact mass data. The signals with the highest intensities found in mass spectrum are *m*/*z* 193.0495 and 149.0233, corresponding to $C_{10}H_9O_4^+$ and $C_8H_5O_3^+$ respectively. Possible structures for some peaks were suggested, helping the construction of reaction pathways that showed the formation of both cyclic monomer and dimer and linear compounds. Typical reactions (intramolecular exchange, via hydroxy-ester and carboxy-ester interchange and six-membered transition state, and intermolecular exchange) have been proposed which may explain the majority of products emitted.

Declaration of Competing Interest

The authors declare that they have no known competing financial interests or personal relationships that could have appeared to influence the work reported in this paper.

Acknowledgements

Access to a EU_FT-ICR_MS network installation funded by the EU Horizon 2020 grant 731077 and support for conducting research is gratefully acknowledged". This work has been funded additionally by Trans National Access (TNA) and LRGP-CNRS, from University of Lorraine. The authors thank Lukas Friederici for his help in SPI and REMPI measurements and Professor René Fournet who provided his expertise on chemical reactions. The authors are grateful to Netzsch Geratebau for using the thermobalances and to German Research Foundation (DFG) for using the Bruker FT-ICR MS.

Appendix A. Supplementary material

Supplementary data to this article can be found online at https://doi.org/10.1016/j.wasman.2020.03.028.

References

Artetxe, M., Lopez, G., Amutio, M., Elordi, G., Olazar, M., Bilbao, J., 2010. Operating conditions for the pyrolysis of poly-(ethylene terephthalate) in a conical spouted-bed reactor. Ind. Eng. Chem. Res. 49, 2064–2069. https://doi.org/10.1021/ie900557c.

Badia, J.D., Martinez-Felipe, A., Santonja-Blasco, L., Ribes-Greus, A., 2013. Thermal and thermo-oxidative stability of reprocessed poly(ethylene terephthalate). J. Anal. Appl. Pyrol. 99, 191–202. https://doi.org/10.1016/j.jaap.2012.09.003.

Bae, E., Na, J.G., Chung, S.H., Kim, H.S., Kim, S., 2010. Identification of about 30 000 chemical components in shale oils by electrospray ionization (ESI) and atmospheric pressure photoionization (APPI) coupled with 15 T fourier transform ion cyclotron resonance mass spectrometry (FT-ICR MS) and a comparison to. Energy Fuels 24, 2563–2569. https://doi.org/10.1021/ef100060b.

Barrow, M.P., Peru, K.M., Headley, J.V., 2014. An added dimension: GC atmospheric pressure chemical ionization FTICR MS and the athabasca oil sands. Anal. Chem. 86, 8281–8288. https://doi.org/10.1021/ac501710y.

Boesl, U., Neusser, H.J., Schlag, E.W., 1978. Two-photon ionization of polyatomic molecules in a mass spectrometer. Zeitschrift für Naturforsch. A 33, 1546–1548. https://doi.org/10.1002/chin.197913069.

Chikh, L., Arnaud, X., Guillermain, C., Tessier, M., Fradet, A., 2003. Cyclizations in hyperbranched aliphatic polyesters and polyamides. Macromol. Symp. 199, 209–221. https://doi.org/10.1002/masy.200350918.

Çit, I., Sinağ, A., Yumak, T., Uçar, S., Misirlioğlu, Z., Canel, M., 2010. Comparative pyrolysis of polyolefins (PP and LDPE)and PET. Polym. Bull. 64, 817–834. https://doi.org/10.1007/s00289-009-0225-x.

Crepier, J., Le Masle, A., Charon, N., Albrieux, F., Duchene, P., Heinisch, S., 2018. Ultra-high performance supercritical fluid chromatography hyphenated to atmospheric pressure chemical ionization high resolution mass spectrometry for the characterization of fast pyrolysis bio-oils. J. Chromatogr. B 1086, 38–46. https://doi.org/10.1016/j.jchromb.2018.04.005.

Czech, H., Schepler, C., Klingbeil, S., Ehlert, S., Howell, J., Zimmermann, R., 2016. Resolving coffee roasting-degree phases based on the analysis of volatile compounds in the roasting off-gas by Photoionization Time-of-Flight Mass Spectrometry (PI-TOFMS) and statistical data analysis: Toward a PI-TOFMS roasting model. Agric. food Chem. 64, 5223–5231. https://doi.org/10.1021/acs.jafc.6b01683.

Czégény, Z., Jakab, E., Blazsó, M., Bhaskar, T., Sakata, Y., 2012. Thermal decomposition of polymer mixtures of PVC, PET and ABS containing brominated flame retardant: formation of chlorinated and brominated organic compounds. J. Anal. Appl. Pyrol. 96, 69–77. https://doi.org/10.1016/j.jaap.2012.03.006.

Czekner, J., Taatjes, C.A., Osbornb, D.L., Meloni, G., 2018. Study of low temperature chlorine atom initiated oxidation of methyl and ethyl butyrate using synchrotron photoionization TOF-mass spectrometry. Phys. Chem. Chem. Phys. 20, 5785–5794. https://doi.org/10.1039/c7cp08221e.

Dayma, G., Thion, S., Lailliau, M., Serinyel, Z., Dagaut, P., Sirjean, B., Fournet, R., 2019. Kinetics of propyl acetate oxidation: Experiments in a jet-stirred reactor, ab initio calculations, and rate constant determination. Proc. Combust. Inst. 37, 429–436. https://doi.org/10.1016/j.proci.2018.05.178.

Deng, Y., Wang, Y.Z., Ban, D.M., Liu, X.H., Zhou, Q., 2006. Burning behavior and pyrolysis products of flame-retardant PET containing sulfur-containing aryl polyphosphonate. J. Anal. Appl. Pyrol. 76, 198–202. https://doi.org/10.1016/j.jaap.2005.11.002.

Dhahak, A., Carré, V., Aubriet, F., Mauviel, G., Burklé-Vitzthum, V., 2020. Analysis of products obtained from slow pyrolysis of Polyethylene Terephthalate by Fourier Transform Ion Cyclotron Resonance Mass Spectrometry coupled to Electrospray Ionization (ESI) and Laser Desorption Ionization (LDI). Ind. Eng. Chem. Res. 59, 1495–1504. https://doi.org/10.1021/acs.iecr.9b05879.

Dhahak, A., Hild, G., Rouaud, M., Mauviel, G., Burkle-Vitzthum, V., 2019. Slow pyrolysis of polyethylene terephthalate: online monitoring of gas production and quantitative analysis of waxy products. J. Anal. Appl. Pyrolysis 142,. https://doi.org/10.1016/j.jaap.2019.104664 104664.

Dorfner, R., Ferge, T., Yeretzian, C., Kettrup, A., Zimmermann, R., 2004. Laser mass spectrometry as on-line sensor for industrial process analysis: process control of coffee roasting. Anal. Chem. 76, 1386–1402. https://doi.org/10.1063/1.1405610.

Dzięcioł, M., Trzeszczyński, J., 2001. Temperature and atmosphere influences on smoke composition during thermal degradation of poly(ethylene terephthalate). J. Appl. Polym. Sci. 81, 3064–3068. https://doi.org/10.1002/app.1757.

Dzięcioł, M., Trzeszczyński, J., 2000. Volatile products of poly(ethylene terephthalate) thermal degradation in nitrogen atmosphere. Appl. Polym. Sci. 77, 1894–1901.

Fendt, A., Geissler, R., Streibel, T., Sklorz, M., Zimmermann, R., 2013. Hyphenation of two simultaneously employed soft photo ionization mass spectrometers with thermal analysis of biomass and biochar. Thermochim. Acta 551, 155–163. https://doi.org/10.1016/j.tca.2012.10.002.

Garozzo, D., Giuffrida, M., Montaudo, G., Lenz, R.W., 1987. Mass spectrometric characterization of poly(ethylene Terephthalate-co-p-Oxybenzoate). J. Polym. Sci. Part A Polym. Chem. 25, 271–284.

Giri, A., Coutriade, M., Racaud, A., Okuda, K., Dane, J., Cody, R.B., Focant, J.F., 2017. Molecular characterization of volatiles and petrochemical base oils by photo-ionization GC×GC-TOF-MS. Anal. Chem. 89, 5395–5403. https://doi.org/10.1021/acs.analchem.7b00124.

Green, C.S., Martin, H., 2006. Fragment-free accurate mass measurement of complex mixture components by gas chromatography/field ionization-orthogonal acceleration time-of-flight mass spectrometry: an unprecedented capability for mixture analysis. Rapid Commun. Mass Spectrom. 15, 236–239. https://doi.org/10.1002/1097-0231(20010215)15:3<236::AID-RCM197>3.0.CO;2-B.

Guo, D.M., Fu, T., Ruan, C., Wang, X.L., Chen, L., Wang, Y.Z., 2015. A new approach to improving flame retardancy, smoke suppression and anti-dripping of PET: Via arylene-ether units rearrangement reactions at high temperature. Polymer (Guildf). 77, 21–31. https://doi.org/10.1016/j.polymer.2015.09.016.

Gupta, Y.N., Chakraborty, A., Pandey, G.D., Setua, D.K., 2004. Thermal and thermooxidative degradation of engineering thermoplastics and life estimation. Appl. Polym. Sci. 92, 1737–1748. https://doi.org/10.1002/app.20134.

Hanley, L., Zimmermann, R., 2009. Light and molecular ions: the emergence of vacuum UV single-photon ionization in MS. Anal. Chem. 81, 4174–4182. https://doi.org/10.1021/ac8013675.

Hsu, H., Ni, C.-K., 2018. Vacuum ultraviolet single-photon postionization of amino acids. Appl. Sci. 8, 1–14. https://doi.org/10.3390/app8050699.

Huang, Q., Liu, C., Wei, R., Wang, J., 2017. Experimental study of polyethylene pyrolysis and combustion over HZSM-5, HUSY, and MCM-41. J. Hazard. Mater. 333, 10–22. https://doi.org/10.1016/j.jhazmat.2017.03.029.

Huba, A.K., Huba, K., Gardinali, P.R., 2016. Understanding the atmospheric pressure ionization of petroleum components: The effects of size, structure, and presence of heteroatoms. Sci. Total Environ. 568, 1018–1025. https://doi.org/10.1016/j.scitotenv.2016.06.044.

Hujuri, U., Ghoshal, A.K., Gumma, S., 2013. Temperature-dependent pyrolytic product evolution profile for polyethylene terephthalate. J. Appl. Polym. Sci. 130, 3993–4000. https://doi.org/10.1002/app.39681.

Jia, L., Le, Y., Brech, Mauviel, G., Qi, F., Fr zowein, M.B., Ehlert, S., Zimmermann, R., Dufour, A., 2016. Online analysis of biomass pyrolysis tar by photoionization mass spectrometry. Energy Fuels 30, 1555–1563. https://doi.org/10.1021/acs.energyfuels.5b02274.

Kai, X., Yang, T., Shen, S., Li, R., 2019. TG-FTIR-MS study of synergistic effects during co-pyrolysis of corn stalk and high-density polyethylene (HDPE). Energy Convers. Manag. 181, 202–213. https://doi.org/10.1016/j.enconman.2018.11.065.

Kamoun, W., Salhi, S., Rousseau, B., El Gharbi, R., Fradet, A., 2006. Furanic-aromatic copolyesters by interchange reactions between poly(ethylene terephthalate) and poly[ethylene 5,5′-isopropylidene-bis(2- furoate)]. Macromol. Chem. Phys. 207, 2042–2049. https://doi.org/10.1002/macp.200600390.

Kawecki, D., Scheeder, P.R.W., Nowack, B., 2018. Probabilistic material flow analysis of seven commodity plastics in Europe. Environ. Sci. Technol. 52, 9874–9888. https://doi.org/10.1021/acs.est.8b01513.

Kekäläinen, T., Venäläinen, T., Jänis, J., 2014. Characterization of birch wood pyrolysis oils by ultrahigh-resolution fourier transform ion cyclotron resonance mass spectrometry: Insights into thermochemical conversion. Energy Fuels 28, 4596–4602. https://doi.org/10.1021/ef500849z.

Kinoshita, R., Teramoto, Y., Yoshida, H., 1993. TG-DTA/FT-IR method for analyzing thermal decomposition mechanism of polyesters. J. Therm. Anal. 40, 605–611. https://doi.org/10.1007/BF02546630.

Kumagai, S., Yamasaki, R., Kameda, T., Saito, Y., Watanabe, A., Watanabe, C., Teramae, N., Yoshioka, T., 2017. Tandem μ-reactor-GC/MS for online monitoring of aromatic hydrocarbon production via CaO- catalysed PET pyrolysis. React. Chem. Eng. 2, 776–784. https://doi.org/10.1039/C7RE00097A.

Lee, J., Lee, T., Tsang, Y.F., Oh, J.I., Kwon, E.E., 2017. Enhanced energy recovery from polyethylene terephthalate via pyrolysis in CO2 atmosphere while suppressing acidic chemical species. Energy Convers. Manag. 148, 456–460. https://doi.org/10.1016/j.enconman.2017.06.026.

Levchik, S.V., Weil, E.D., 2004. A review on thermal decomposition and combustion of thermoplastic polyesters. Polym. Adv. Technol. 15, 691–700. https://doi.org/10.1002/pat.526.

Li, D.X., Gan, L., Bronja, A., Schmitz, O.J., 2015. Gas chromatography coupled to atmospheric pressure ionization mass spectrometry (GC-API-MS): review. Anal. Chim. Acta 891, 43–61. https://doi.org/10.1016/j.aca.2015.08.002.

Li, X., Sun, G., Chen, S., Fang, Z., Yuan, H., Shi, Q., Zhu, Y., 2018. Molecular chemodiversity of dissolved organic matter in paddy soils. Environ. Sci. Technol. 52, 963–971. https://doi.org/10.1021/acs.est.7b00377.

Miettinen, I., Kuittinen, S., Paasikallio, V., Mäkinen, M., Pappinen, A., Jänis, J., 2017. Characterization of fast pyrolysis oil from short-rotation willow by high-resolution Fourier transform ion cyclotron resonance mass spectrometry. Fuel 207, 189–197. https://doi.org/10.1016/j.fuel.2017.06.053.

Montaudo, G., Puglisi, C., Samperi, F., 1993. Primary thermal degradation mechanisms of PET and PBT. Polym. Degrad. Stab. 42, 13–28. https://doi.org/10.1016/0141-3910(93)90021-A.

Murillo, E.A., Vallejo, P.P., López, B.L., 2010. Characterization of hydroxylated hyperbranched polyesters of fourth and fifth generation. E-Polymers 10, 1347–1358. https://doi.org/10.1515/epoly.2010.10.1.1347.

Nasser, A.L.M., Lopes, L.M.X., Eberlin, M.N., Monteiro, M., 2005. Identification of oligomers in polyethyleneterephthalate bottles for mineral water and fruit juice development and validation of a high-performance liquid chromatographic method for the determination of first series cyclic trimer. J. Chromatogr. A 1097, 130–137. https://doi.org/10.1016/j.chroma.2005.08.023.

NIST Chemistry webbook [Gas phase ion energetics data] Available online : (last accessed Mai 2019) [WWW Document], n.d. (https://webbook.nist.gov/chemistry/)

Ohtani, H., Kimura, T., Tsuge, S., 1986. Analysis of thermal by high-resolution degradation of terephthalate chromatography. Anal. Sci. 2, 179–182.

Oni, O., Schmidt, F., Miyatake, T., Kasten, S., Friedrich, M.W., 2015. Microbial communities and organic matter composition in surface and subsurface sediments of the helgoland mud area. North Sea. Front. Microbiol. 6, 1290. https://doi.org/10.3389/fmicb.2015.01290.

Pan, Y., Wang, W., Pan, H., Zhan, J., Hu, Y., 2016. Fabrication of montmorillonite and titanate nanotube based coatings: Via layer-by-layer self-assembly method to enhance the thermal stability, flame retardancy and ultraviolet protection of polyethylene terephthalate (PET) fabric. RSC Adv. 6, 53625–53634. https://doi.org/10.1039/c6ra05213d.

Parr, M.K., Wüst, B., Teubel, J., Joseph, J.F., 2018. Splitless hyphenation of SFC with MS by APCI, APPI, and ESI exemplified by steroids as model compounds. J. Chromatogr. B 1091, 67–78. https://doi.org/10.1016/j.jchromb.2018.05.017.

Plage, B., Schulten, H.R., 1990. Thermal degradation and mass spectrometric fragmentation processes of polyesters studied by time-/temperature-resolved pyrolysis-field ionization mass spectrometry. Macromolecules 23, 2642–2648. https://doi.org/10.1021/ma00212a008.

Qian, K., Dechert, G.J., 2002. Recent advances in petroleum characterization by GC field ionization time-of-flight high-resolution mass spectrometry. Anal. Chem. 74, 3977–3983. https://doi.org/10.1021/ac020166d.

Rüger, C.P., Grimmer, C., Sklorz, M., Neumann, A., Streibel, T., Zimmermann, R., 2018. Combination of different thermal analysis methods coupled to mass spectrometry for the analysis of asphaltenes and their parent crude oils: comprehensive characterization of the molecular pyrolysis pattern. Energy Fuels 32, 2699–2711. https://doi.org/10.1021/acs.energyfuels.7b02762.

Rüger, C.P., Miersch, T., Schwemer, T., Sklorz, M., Zimmermann, R., 2015. Hyphenation of thermal analysis to ultrahigh-resolution mass spectrometry (fourier transform ion cyclotron resonance mass spectrometry) using atmospheric pressure chemical ionization for studying composition and thermal degradation of complex materials. Anal. Chem. 87, 6493–6499. https://doi.org/10.1021/acs.analchem.5b00785.

Samperi, F., Puglisi, C., Alicata, R., Montaudo, G., 2004. Thermal degradation of poly (ethylene terephthalate) at the processing temperature. Polym. Degrad. Stab. 83, 3–10. https://doi.org/10.1016/S0141-3910(03)00166-6.

Saraji-Bozorgzad, M., Geissler, R., Streibel, T., Mühlberger, F., Sklorz, M., Kaisersberger, E., Denner, T., Zimmermann, R., 2008. Thermogravimetry coupled to single photon ionization quadrupole mass spectrometry: A tool to investigate the chemical signature of thermal decomposition of polymeric materials. Anal. Chem. 80, 3393–3403. https://doi.org/10.1021/ac702599y.

Shi, Z., Jin, L., Zhou, Y., Li, H., Li, Y., Hu, H., 2018. In-situ analysis of catalytic pyrolysis of Baiyinhua coal with pyrolysis time-of-flight mass spectrometry. Fuel 227, 386–393. https://doi.org/10.1016/j.fuel.2018.04.109.

Sophonrat, N., Sandström, L., Johansson, A.C., Yang, W., 2017. Co-pyrolysis of mixed plastics and cellulose: an interaction study by Py-GC×GC/MS. Energy Fuels 31, 11078–11090. https://doi.org/10.1021/acs.energyfuels.7b01887.

Sovová, K., Ferus, M., Matulková, I., Španěl, P., Dryahina, K., Dvořák, O., Civiš, S., 2008. A study of thermal decomposition and combustion products of disposable polyethylene terephthalate (PET) plastic using high resolution fourier transform infrared spectroscopy, selected ion flow tube mass spectrometry and gas chromatography mass spectrometr. Mol. Phys. 106, 1205–1214. https://doi.org/10.1080/00268970802077876.

Fukuzawa, T., Tanimizu, S., 1978. Flourescence decay characteristics of Tb3+-activated phosphates under H2-VUV laser excitation. J. Lumin. 16, 447–456.

Taylor, R., 1983. The mechanism of thermal elimination. Part 17. rate data for pyrolysis of vinyl acetate and 1,2-diacetoxyethane. J. Chem. Soc. Perkin Trans. 2 0, 1157–1160.

Tose, L.V., Cardoso, F.M.R., Fleming, F.P., Vicente, M.A., Silva, S.R.C., Aquije, G.M.F.V., Vaz, B.G., Romão, W., 2015. Analyzes of hydrocarbons by atmosphere pressure chemical ionization FT-ICR mass spectrometry using isooctane as ionizing reagent. Fuel 153, 346–354. https://doi.org/10.1016/j.fuel.2015.03.004.

Trukhin, A.N., Golant, K.M., 2009. Peculiarities of photoluminescence excited by 157 nm wavelength F2 excimer laser in fused and unfused silicon dioxide. J. Non. Cryst. Solids 355, 1719–1725. https://doi.org/10.1016/j.jnoncrysol.2009.06.020.

Turnbull, L., Liggat, J.J., Macdonald, W.A., 2013. Thermal degradation chemistry of poly(ethylene naphthalate) - a study by thermal volatilisation analysis. Polym. Degrad. Stab. 98, 2244–2258. https://doi.org/10.1016/j.polymdegradstab.2013.08.018.

Ubeda, S., Aznar, M., Nerín, C., 2018. Determination of oligomers in virgin and recycled polyethylene terephthalate (PET) samples by UPLC-MS-QTOF. Anal. Bioanal. Chem. 410, 2377–2384. https://doi.org/10.1007/s00216-018-0902-4.

Van Dam, H., Oskam, A., 1978. He(I) and He(II) photoelectron spectra of some substituted ethylenes. J. Electron Spectros. Relat. Phenomena 13, 273–290.

Wang, Y., Huang, Q., Zhou, Z., Yang, J., Qi, F., Pan, Y., 2015. Online study on the pyrolysis of polypropylene over the HZSM-5 zeolite with photoionization time-of-flight mass spectrometry. Energy Fuels 29, 1090–1098.

Wu, Q., Hua, L., Hou, K., Cui, H., Chen, W., Chen, P., Wang, W., Li, J., Li, H., 2011. Vacuum ultraviolet lamp based magnetic field enhanced photoelectron ionization and single photon ionization source for online time-of-flight mass spectrometry. Anal. Chem. 83, 8992–8998. https://doi.org/10.1021/ac201791n.

Xu, J., Zhuo, J., Zhu, Y., Pan, Y., Yao, Q., 2017. Analysis of volatile organic pyrolysis products of bituminous and anthracite coals with single-photon ionization time-of-flight mass spectrometry and gas chromatography/mass spectrometry. Energy Fuels 31, 730–737. https://doi.org/10.1021/acs.energyfuels.6b02335.

Yoshioka, T., Grause, G., Eger, C., Kaminsky, W., Okuwaki, A., 2004. Pyrolysis of poly (ethylene terephthalate) in a fluidised bed plant. Polym. Degrad. Stab. 86, 499–504. https://doi.org/10.1016/j.polymdegradstab.2004.06.001.

Yuzawa, T., Watanabe, C., Nemoto, N., Ohtani, H., 2013. Rapid evaluation of photo, thermal and oxidative degradation of high impact polystyrene by a xenon lamp-based online ultraviolet irradiation-pyrolysis-GC/MS system. Polym. Degrad. Stab. 98, 671–676. https://doi.org/10.1016/j.polymdegradstab.2012.11.005.

Zander, N.E., Gillan, M., Lambeth, R.H., 2018. Recycled polyethylene terephthalate as a new FFF feedstock material. Addit. Manuf. 21, 174–182. https://doi.org/10.1016/j.addma.2018.03.007.

Zhou, Z., Chen, X., Wang, Y., Liu, C., Ma, H., Zhou, C., 2019. Bioresource technology online photoionization mass spectrometric evaluation of catalytic co- pyrolysis of cellulose and polyethylene over HZSM-5. Bioresour. Technol. 275, 130–137. https://doi.org/10.1016/j.biortech.2018.12.045.

Zimmermann, R., Heger, H.J., Kettrup, A., 1999. On-line monitoring of traces of aromatic-, phenolic- and chlorinated components in flue gases of industrial scale incinerators and cigarette smoke by direct-inlet laser ionization-mass spectrometry (REMPI-TOFMS). Fresenius. J. Anal. Chem. 363, 720–730. https://doi.org/10.1007/s002160051281.